Successive phase transitions driven by orbital ordering and electron transfer in quasi-two-dimensional $CrSe_2$ with a triangular lattice

Shintaro Kobayashi,[1] Hiroaki Ueda,[1] Daisuke Nishio-Hamane,[2] Chishiro Michioka,[1] and Kazuyoshi Yoshimura[1]

[1]*Department of Chemistry, Graduate School of Science, Kyoto University, Kyoto 606-8502, Japan*

[2]*Institute for Solid State Physics, The University of Tokyo, Chiba 277-8581, Japan*

(Received 26 July 2013; revised manuscript received 4 January 2014; published 12 February 2014)

We report physical properties of a chromium dichalcogenide 1T-$CrSe_2$ with tetravalent Cr cations. Interplay between orbital degrees of freedom and the valence instability of Cr is studied by means of magnetic, electrical, electron diffraction, and x-ray diffraction measurements. Associated with the phase transitions, a space group of $CrSe_2$ varies from trigonal $P\bar{3}m1$ to rhombohedral $R\bar{3}m$ through monoclinic $I2/m$. By considering behaviors of χ and ρ in addition to possible ordering patterns of occupied t_{2g} orbitals, we have concluded that the origin of successive phase transitions is simultaneous occurrence of orbital ordering and valence change of Cr through each phase transition.

DOI: 10.1103/PhysRevB.89.054413 PACS number(s): 75.25.Dk, 61.05.cp, 71.20.Be

I. INTRODUCTION

Layered transition metal dichalcogenides MX_2 (M = transition metal, X = chalcogen) are of much interest due to their wide variety of electric, magnetic, and optical properties and especially their structural phase transitions. Among them, 1T-MX_2 compounds are a series of quasi-two-dimensional compounds with a triangular lattice, and they often exhibit a charge density wave (CDW) caused by their electronic instability of a two-dimensional structure. For example, 1T-$TiSe_2$ and 1T-VSe_2 with tetravalent transition metal ions show successive phase transitions accompanied by periodic lattice distortions coupled with CDW [1,2].

Another tetravalent transition metal selenide, 1T-$CrSe_2$, was also reported to show successive phase transitions [3]. However, the origin of phase transitions remains unknown. According to a previous report [3], magnetic susceptibility increases stepwise at 186 K and 164 K with decreasing temperature, and electrical resistivity has almost no anomaly at these temperatures. These behaviors are different from those expected from a CDW picture. In addition, the recent study of substitution effects [4] suggests that the ground state of $CrSe_2$ is not CDW but possibly an antiferromagnetically ordered state.

We suspect that these successive phase transitions of $CrSe_2$ originate from the unusual nature of tetravalent Cr ions. In $CrSe_2$, the formal valence of Cr ions is +4, assuming the Se valence of −2. Indeed, x-ray absorption spectra at room temperature [5] suggest that $CrSe_2$ belongs to a family of d^2-type compounds despite a strong overlap of Cr 3d and Se 4p bands [6]. However, the role of Cr^{4+} in the physical properties of $CrSe_2$ is not yet fully recognized and understood.

Compared with highly stable Cr^{3+} with a half-filled t_{2g} level, Cr^{4+} is relatively unstable and has a tendency to become Cr^{3+}. This electronic instability of tetravalent chromium compounds can be visualized as negative charge transfer energy within the framework of the Zaanen-Sawatzky-Allen (ZSA) scheme [7,8]. For example, band calculations suggest that a metallic ferromagnet, CrO_2, belongs to this class of materials [9–11]. Tetravalent chromium compounds often exhibit a variety of unconventional physical properties originating from an unstable electronic state. Due to such electronic instability, tetravalent chromium compounds often exhibit a variety of unconventional physical properties, such as a colossal magnetoresistive effect of $NaCr_2O_4$ [12] and a metal-to-insulator transition of $K_2Cr_8O_{16}$ in a ferromagnetic state [13].

In addition, Cr^{4+} has orbital degrees of freedom with an electron configuration of t_{2g}^2. It is well known that transition metal compounds with orbital degeneracy often demonstrate structural transitions accompanied by orbital ordering in order to remove orbital degeneracy. Particularly, if transition metals with orbital degeneracy are on a geometrically frustrated lattice, such as triangular and pyrochlore lattices, unconventional orbital ordering patterns are often observed. For systems on a pyrochlore lattice, heptamer clusters in AlV_2O_4 [14], helical dimers in $MgTi_2O_4$ [15], and octamer clusters in $CuIr_2S_4$ [16,17] were reported. Triangular lattice compounds $LiVO_2$ [18,19] and $LiVS_2$ [20] have the same electron configuration of t_{2g}^2 as $CrSe_2$, and trimer clusters are observed in their ordered states. Similarly, unconventional structural changes with orbital ordering can be expected in $CrSe_2$, since it has orbital degrees of freedom on a triangular lattice.

Here we report detailed physical properties of $CrSe_2$ and discuss the origin of successive phase transitions. We found successive structural changes and superlattice formation, suggesting orbital ordering. We also propose possible orbital ordering patterns of low-temperature phases. We conclude that a two-step electron transfer from Se to Cr and the formation of Cr^{3+} induce successive phase transitions.

II. EXPERIMENTS

Polycrystalline samples of $CrSe_2$ were prepared through deintercalation of K from K_xCrSe_2 ($x \approx 0.9$) with iodine in acetonitrile, as previously reported [3]. Single crystals of $CrSe_2$ were obtained, using this same deintercalation procedure, from K_xCrSe_2 single crystals grown by a KBr-KI flux method.

These samples were characterized by powder x-ray diffraction (XRD) on a diffractometer (M18XHF, Mac Science) with Cu$K\alpha$ radiation. Polycrystalline samples were measured in Debye-Scherrer geometry after they were loosely loaded in a 2-mm-diameter borosilicate glass capillary in order to avoid preferred orientation effects. Single crystals oriented

on a glass plate were measured in Bragg-Brentano geometry. Low-temperature XRD measurements were performed using polycrystalline samples in Bragg-Brentano geometry with a closed-cycle refrigerator.

Electron diffraction measurements were carried out using a transmission electron microscope (JEM-2010F, JEOL) with a liquid nitrogen cooling system. The chemical composition of polycrystalline samples was determined using inductively coupled plasma spectrometry (JY138KH, Horiba), and that of single crystals was analyzed using energy-dispersive x-ray spectroscopy (JED-2200, JEOL). The magnetic susceptibility was measured using a superconducting quantum interference device magnetometer (MPMS, Quantum Design). For the susceptibility measurements of single crystals, approximately 100 small single crystals were aligned on a PET film and the magnetic field was applied parallel or perpendicular to the c axis. Electrical resistivity of single crystals was measured perpendicular to the c axis using a conventional four-probe method.

III. RESULTS AND DISCUSSION

A. Synthesis and characterization

$CrSe_2$ is not known to be obtained using solid-state reactions. As previously reported [3], we synthesized polycrystalline samples of $CrSe_2$ through a deintercalation process. In addition, we succeeded in obtaining single crystals of $CrSe_2$ for the first time. As shown in the inset of Fig. 1, obtained single crystals of $CrSe_2$ are black hexagonal platelets with a typical size of $0.3 \times 0.3 \times 0.1$ mm. However, these single crystals have many cracks and are quite fragile. We think this is due to a large strain caused by deintercalation of K with a large ionic radius.

In the main panel of Fig. 1, XRD patterns of a polycrystalline sample and single crystals are shown with a simulated profile. The XRD pattern of the polycrystalline sample agrees with the simulated one, which indicates that our sample is in a single phase of 1T-$CrSe_2$ with a space group of $P\bar{3}m1$. By fitting the data, the lattice parameters are found to be $a = 3.40$ Å and $c = 5.91$ Å. The XRD pattern of single crystals shows large 0 0 l Bragg peaks, and their positions are quite consistent with the lattice parameter c, suggesting successful synthesis of single crystals of $CrSe_2$.

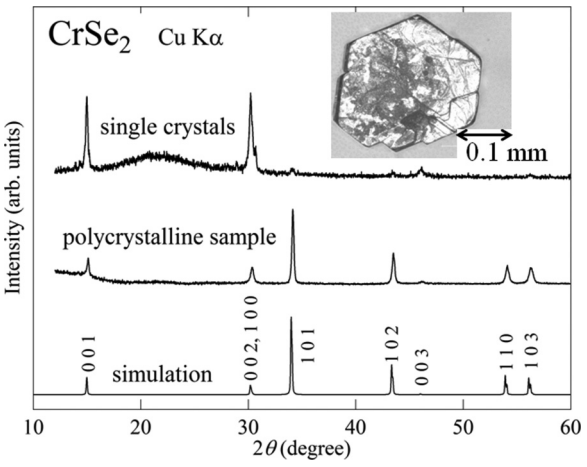

FIG. 1. X-ray diffraction patterns of single crystals, polycrystalline samples, and a simulated profile of $CrSe_2$. Numbers above the simulated profile designate indices of each diffraction. The inset shows a photograph of a single crystal.

A chemical composition of polycrystalline samples gives a ratio of $Se/Cr \simeq 1.97(3)$, and that of single crystals gives a ratio of 2.00(4). These values indicate that our samples are almost stoichiometric. No trace of K is detected in our measurements, implying that complete deintercalation of K is achieved.

B. Magnetic susceptibility

In a previous study [3], magnetic susceptibility shows two anomalies associated with phase transitions around 186 K and 164 K. The top panel of Fig. 2 shows the temperature dependence of the magnetic susceptibility $\chi = M/H$ of our polycrystalline samples, where M is the magnetization and H is the magnetic field. Despite slightly different transition temperatures, our data are qualitatively similar to data of the previous report. With decreasing temperature, χ slightly decreases and increases stepwise at $T_{t1} \simeq 190$ K and $T_{t2} \simeq 170$ K successively. Below T_{t2}, χ starts to decrease again. Both two-phase transitions are of the first order, since χ shows clear temperature hystereses, as shown in the left inset

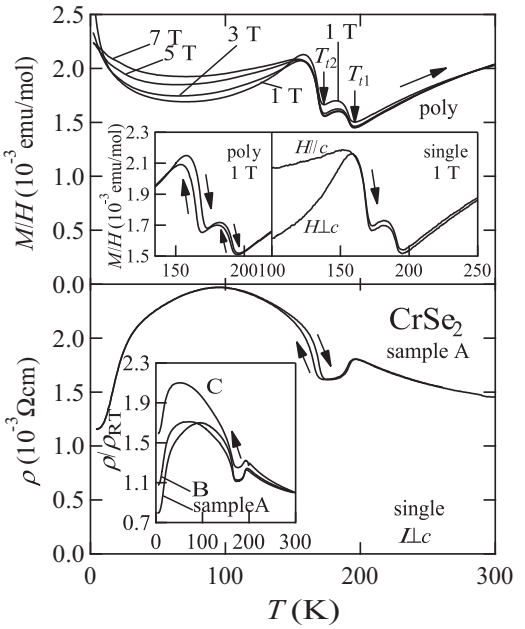

FIG. 2. Magnetic susceptibility and electrical resistivity of $CrSe_2$ as a function of temperature. The top panel shows the magnetic susceptibility of a polycrystalline sample at various magnetic fields. The left inset shows a magnification of the susceptibility around the transition temperatures, which indicates temperature hystereses. The right inset shows the magnetic susceptibility of single crystals with the field parallel or perpendicular to the c axis. The bottom panel shows electrical resistivity of a single crystal. The inset shows sample dependence of electrical resistivity with the data normalized to unity at room temperature. The measurements of magnetic susceptibility and electrical resistivity were performed in both cooling and heating processes, which are indicated by arrows.

of the top panel of Fig. 2 and heat absorptions on warming are observed at both transition temperatures in a differential scanning calorimetry measurement [3]. The clear steps of χ at T_{t1} and T_{t2} suggest drastic changes of the spin state at these transitions.

In a low-temperature region, χ shows a Curie tail, which corresponds to 0.85% of Cr^{4+} local moments ($S = 1$). The magnitude of this Curie tail is very small and sample dependent, which strongly suggests it is extrinsic. The Curie tail in our sample is much smaller than that in the previous report [3,4], indicating the good quality of our sample.

As shown in the figure, M/H below T_{t1} has field dependence. Below T_{t2}, field dependence is more distinct and M/H becomes gradually larger by applying a magnetic field up to 7 T. In addition, χ of single crystals exhibits large anisotropy especially below T_{t2}, as shown in the right inset of the top panel of Fig. 2. These behaviors give us important information on the spin state of $CrSe_2$. At least below T_{t2}, $CrSe_2$ likely has localized magnetic moments, and the moments are ordered perpendicular to the c axis. The field dependence of χ of a polycrystalline sample is possibly due to a spin-flop transition which is observed in the typical magnetization process of antiferromagnets. The existence of localized magnetic moments is consistent with the relatively large value of χ of about 2×10^{-3} emu/mol. Indeed, chromium selenides with localized Cr^{3+} moments have almost the same order of χ. For example, Cr_2Se_3 has χ of about 4×10^{-3} emu/Cr mol [21].

In spite of the little magnetic anisotropy and the absence of field dependence of M/H above T_{t1}, the magnitude of M/H above T_{t1} is comparable to that below T_{t1}, implying that d electrons in Cr are almost localized. The value of χ above T_{t1} is much larger than the values of typical transition metal dichalcogenides with Pauli paramagnetism. For example, χ of 1T-VSe_2 is about 3×10^{-4} emu/mol at 300 K [22]. In addition, χ of $CrSe_2$ has a large temperature dependence above T_{t1}. The increase of χ with rising temperature is inconsistent with the temperature-independent Pauli paramagnetism. Since this temperature dependence is similar to those of antiferromagnets below Néel temperature, one possibility is that $CrSe_2$ is antiferromagnetically ordered even above T_{t1}, which is suggested by a band calculation with and without spin polarization [6].

C. Transport property

As discussed above, rapid changes of χ at T_{t1} and T_{t2} suggest that the spin state successively varies in the magnetically ordered state. If those transitions are simple magnetic phenomena, the effect on electrical resistivity ρ is expected to be small. In the previous study [3], ρ of a powder compact sample shows no anomaly around T_{t1} and T_{t2}. In contrast, our ρ data of single crystals exhibit two clear anomalies at T_{t1} and T_{t2}, as shown in the bottom panel of Fig. 2. With a temperature decreasing from room temperature, ρ slightly increases down to T_{t1} and abruptly decreases at T_{t1}. Between T_{t1} and T_{t2}, ρ is almost constant, but it drastically increases at T_{t2}. Below T_{t2}, ρ increases and goes through the maximum at around 90 K and then decreases monotonically to the lowest temperature. In a low-temperature region, ρ exhibits a metallic behavior, which is completely different from the previously reported semiconducting behavior [3]. Our observation indicates drastic changes of electronic states in addition to spin-state changes at these phase transitions.

However, our ρ data show sample dependence to a certain extent, as shown in the inset of the bottom panel of Fig. 2, which is likely due to cracks. For example, while sample A has the maximum in ρ at approximately 90 K, sample C has the maximum in ρ at around 50 K. With more cracks, it seems that the value of ρ becomes larger and that the temperature dependence becomes semiconducting. Then the residual-resistivity ratio RRR $= \rho_{300K}/\rho_{0K}$ becomes smaller. Despite the little difference in RRR, all our ρ data show two clear anomalies and a metallic behavior, which indicates the intrinsic behavior of ρ.

The behavior of ρ can be compared with the results of previous band structure calculations [6]. According to the results, $CrSe_2$ is a magnetic metal with large density of states at the Fermi level. This is because not only the wide Se band but also the narrow Cr band lies at the Fermi level. The large contribution of Cr at the Fermi level suggests that $CrSe_2$ is likely a strongly correlated electron system. This interpretation is consistent with the large value of ρ and the semiconducting behavior above T_{t1} in our data. Meanwhile, these band structure calculations are based on the crystal structure at room temperature, and they give no explanation about the phase transitions.

Now we consider the origin of the phase transitions. These magnetic and electrical behaviors of $CrSe_2$ are not explained with the CDW of the conduction band. The changes of χ and ρ through the transitions are not consistent with the typical behavior with CDW transitions, in which ρ increases and χ decreases due to the reduction of the density of states with the formation of CDW. Taking this into account, the origin of phase transitions of $CrSe_2$ is not due to simple CDW instability. Since χ jumps at these transitions, it is natural to expect that electronic states of Cr atoms are closely related to the origin of these phase transitions. Considering the orbital degeneracy of the Cr atoms above T_{t1}, orbital ordering likely takes place at these phase transitions. The details are discussed later.

D. Low-temperature structures

The previous report [3] suggests that $CrSe_2$ shows a structural transition at T_{t1}. However, the structure in a low-temperature region is not clarified. It is important to know the detailed structure in a low-temperature region to elucidate the origin of the phase transitions. In order to study the details of phase transitions from a structural viewpoint, we conducted powder XRD measurements at low temperatures, and we found successive structural changes accompanied by superlattice formation.

As shown in Fig. 3(a), the cell volume V, the lattice parameters a and c change markedly at T_{t1}, which is consistent with the previous report [3]. With decreasing temperature, a decreases and c increases in the high-temperature (HT) phase ($T_{t1} < T$). At T_{t1}, a increases and c decreases stepwise. While a slightly decreases below T_{t1} through T_{t2}, c is almost constant in the intermediate-temperature (IT) phase ($T_{t2} < T < T_{t1}$) and decreases monotonically in the low-temperature (LT)

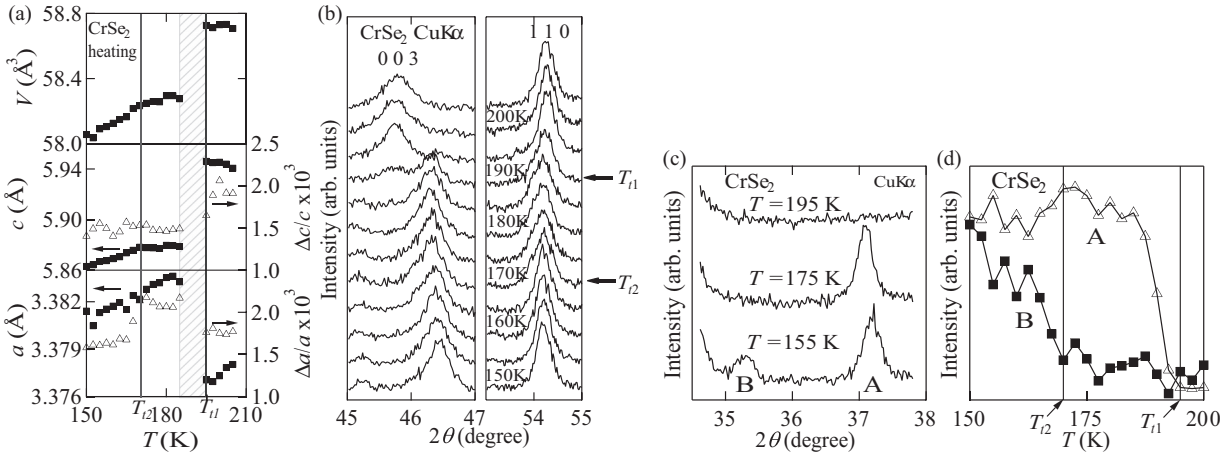

FIG. 3. (a) Temperature dependence of the unit cell volume V, the lattice parameters a and c (solid squares), and normalized deviation of lattice parameters $\Delta a/a$ and $\Delta c/c$ (open triangles). Δa and Δc are evaluated from the 1 1 0 peak and the 0 0 3 peak, respectively. Between 185 K and 193 K, these parameters could not be determined because of the coexistence of HT and IT phases. (b) Temperature dependence of the shapes of the 1 1 0 peak and the 0 0 3 peak. (c) Temperature dependence of XRD patterns measured at various temperatures. The XRD data of the upper, middle, and lower curves correspond to those measured in the HT, IT, and LT phases, respectively. (d) Temperature dependence of the superlattice reflection intensities around 37.2° (A, open triangles) and 35.2° (B, solid squares). The intensity of B becomes almost zero above T_{t2}; in contrast, that of A diminishes above T_{t1}.

phase ($T < T_{t2}$). Roughly speaking, a large structural change occurs at T_{t1}, and a small change seems to take place at T_{t2}.

At T_{t2}, a significant change is not detected in a but in a normalized deviation of the lattice parameter $\Delta a/a$, as shown in Fig. 3(a). Deviations of lattice parameter Δa and Δc are calculated from full width at half maximum of the 1 1 0 peak and the 0 0 3 peak, respectively. Temperature dependence of the shapes of the 1 1 0 peak and the 0 0 3 peak is shown in Fig. 3(b). $\Delta a/a$ in the IT phase is clearly larger than those in the HT and LT phases, while $\Delta c/c$ in the IT phase is smaller than that in the HT phase and is almost the same as that in the LT phase. This enhancement of $\Delta a/a$ in the IT phase is not due to coexistence of the IT and HT phases, since $\Delta c/c$ in the IT phase is smaller than that in the HT phase. Of course, this increase does not originate from coexistence of the IT and LT phases, since a hardly changes between these two phases. Hence, the increase of $\Delta a/a$ seemingly indicates $a \neq b$ in the IT phase. Therefore, the IT phase is a monoclinic or triclinic crystal system, which is discussed later. In the LT phase, $\Delta a/a$ is almost the same as that of the HT phase, indicating that $a = b$. A small but obvious structural change occurs even at T_{t2}.

In addition, we successfully found superlattice reflections in both the IT and LT phases. About a dozen superlattice reflections were observed in our XRD studies. Their positions are the same for both the IT and the LT phases, and their intensities are different between these phases, indicating that $CrSe_2$ has the same translational symmetry but different superstructures in the IT and LT phases. Typical examples of superlattice reflections are exhibited in Fig. 3(c). In this region, the LT phase has two superlattice peaks A and B around 37.2° and 35.2°, respectively. In the IT phase, while peak A seems to become large, peak B almost vanishes. The temperature dependence of the peak intensity of these superlattice peaks is plotted in Fig. 3(d). With increasing temperature, the intensity of B becomes almost zero at T_{t2}, while that of A slightly increases at T_{t2} and becomes zero at T_{t1}. In the present stage, we cannot determine the indices of these superlattice peaks in these measurements.

In order to determine the details of superlattices in the LT phase, electron diffraction measurements were carried out. In these measurements, superlattice reflections are well indexed, as shown in Fig. 4. At 90 K, electron diffraction patterns show superlattice reflections at $h/3$ $k/3$ $l/3$-type positions in addition to fundamental spots observed at 300 K.

Considering the extinction rule, we determined that the LT phase of $CrSe_2$ has a rhombohedral structure with a space group of $R\bar{3}m$ with a $3a \times 3b \times 3c$ supercell in hexagonal axes. This space group is a subgroup of $P\bar{3}m1$, a space group of the HT phase. The above-mentioned XRD patterns in the LT phase are quite consistent with a space group of $R\bar{3}m$.

As discussed above, two-phase transitions do not originate from the CDW, and it is likely that orbital orderings of Cr^{4+} with t_{2g}^2 involve these transitions. Structural changes and superstructure formation observed in XRD and electron diffraction measurements are quite consistent with orbital ordering. Before we examine a possible orbital ordering pattern, we discuss changes of atomic positions of Cr in the LT phase. In the LT phase, $CrSe_2$ has three Cr sites—Cr1 (0, 0, 0), Cr2 (0, 0, $1/3 + z$), and Cr3 ($1/3 + x$, 0, 0)—based on a space group of $R\bar{3}m$ in hexagonal axes. Considering the layered structure of $CrSe_2$, we simply focus on the atomic positions within the ab plane. Then, the following two models are possible. The first one is a hexamer model with $x < 0$, displayed in Fig. 5(a), in which Cr3 atoms approach neighboring Cr1 atoms. The second is a dimer model with $x > 0$. In this model, each Cr3 atom goes away from a neighboring Cr1 atom and gets closer to a neighboring Cr3 atom.

These changes of atomic positions are closely related to the orbital ordering of Cr. Now, we consider orbital ordering patterns of the LT phase, which satisfy a space group of $R\bar{3}m$. In the presence of a threefold rotation axis through

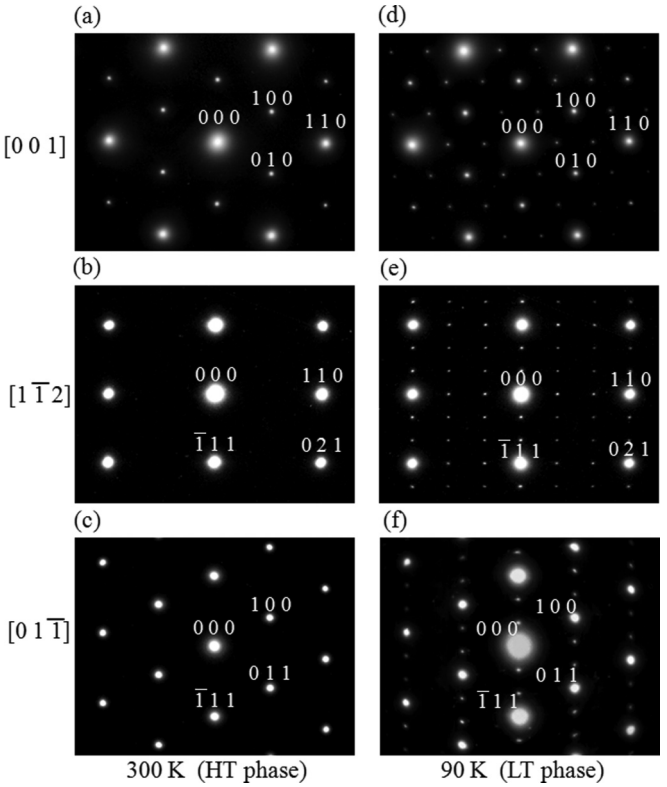

FIG. 4. Electron diffraction patterns of $CrSe_2$ (a) at 300 K with [0 0 1] incidence, (b) at 300 K with [1 $\bar{1}$ 2] incidence, (c) at 300 K with [0 1 $\bar{1}$] incidence, (d) at 90 K with [0 0 1] incidence, (e) at 90 K with [1 $\bar{1}$ 2] incidence, and (f) at 90 K with [0 1 $\bar{1}$] incidence. At 90 K, a set of superlattice spots with $h/3\ k/3\ l/3$-type indices appears in addition to fundamental spots.

a Cr atom, three t_{2g} orbitals are equivalent, since they are interchanged in this threefold rotation. In this case, d electrons of Cr are considered to occupy three t_{2g} orbitals with the same proportion. Indeed, the HT phase with a space group of $P\bar{3}m1$ has threefold rotation axes through all Cr atoms, and it has an orbital disordered state. In contrast, the LT phase with a space group of $R\bar{3}m$ has threefold rotation axes through Cr1 and Cr2, but it does not have them through Cr3. Although these threefold

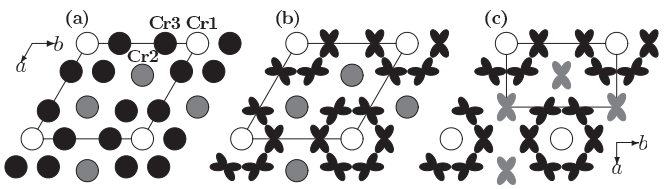

FIG. 5. Schematic views of (a) atomic positions of Cr atoms in a hexamer model of the LT phase, (b) an orbital ordering pattern of the LT phase, and (c) an orbital ordering pattern of the IT phase are drawn within the hexagonal ab plane. Solid lines express the unit cells. In (a) and (b), the LT phase has the $3a \times 3b \times 3c$ hexagonal unit cell with a space group of $R\bar{3}m$. In (c), the monoclinic unit cell of the IT phase with a space group of $I2/m$ has the same lattice vectors $\boldsymbol{b}$ and $\boldsymbol{c}$ as those of the LT phase. Please note that the a axis in (c) is not parallel to the hexagonal ab plane. The LT phase has three inequivalent Cr sites—Cr1, Cr2, and Cr3—which are represented using white, gray, and black colors, respectively. In the orbital ordering patterns of (b) and (c), only in-plane lobes with an electron are displayed.

rotation axes through Cr1 and Cr2 indicate equivalence of three t_{2g} orbitals of Cr1 and Cr2, the absence of a threefold rotation axis strongly suggests that t_{2g} orbitals of Cr3 are ordered. Focusing on threefold rotation axes through Cr1 and Cr2, only one orbital ordering pattern of Cr3 is possible, which is shown in Fig. 5(b).

E. Origin of successive phase transitions

We have proposed a possible orbital ordering pattern of the LT phase. However, this model has some shortcomings. As mentioned above, orbital states of unclustered Cr1 and Cr2 seem to remain disordered even in the ground state. In addition, this model seems inconsistent with physical properties such as χ and ρ, and it gives no explanation for the two-step nature of these transitions. By considering these unclustered Cr atoms, these shortcomings are reasonably resolved, as described below.

Although drastic increases of χ at T_{t1} and T_{t2} by lowering temperature are seemingly inconsistent with the formation of orbital ordering, unclustered Cr ions possibly cause increases of χ. In many t_{2g} orbital ordered systems, χ reduces accompanied by orbital ordering due to spin-singlet formation. However, some compounds show an increase of χ with orbital ordering. For example, in an orbital ordered state of $BaV_{10}O_{15}$, χ is enhanced by small magnetic interactions between unclustered V ions, even though the number of spins reduces due to the formation of V clusters [23]. $CrSe_2$ has two unclustered Cr sites (Cr1 and Cr2), which do not form spin singlets. These unclustered Cr atoms are a key to understanding the increases of χ. As the origin of increases of χ despite the reduction of the number of spins, the following two types of spin-state changes of unclustered Cr are possible. One is a change of magnetic interaction, which is similar to $BaV_{10}O_{15}$, and/or a change of magnetically ordered pattern. The other is a change of magnitude of magnetic moments of unclustered Cr atoms. However, in the former case, changes of magnetic interaction and/or spin structures have little effect on ρ. Consequently, the origin of characteristic behaviors of χ and ρ at phase-transition temperatures is not only due to a change of magnetic interactions and/or magnetic structures but also due to a change of the magnitude of magnetic moments of unclustered Cr.

Here we discuss the orbital states of unclustered Cr1 and Cr2 in the LT phase based on the symmetry. In the LT phase, Cr1 and Cr2 have threefold rotation axes which make three t_{2g} orbitals equivalent. These Cr atoms have two possible orbital states with equivalent t_{2g} orbitals. One is the state in which occupied t_{2g} orbitals are disordered. In this case, the orbital of Cr3 is ordered and those of Cr1 and Cr2 are disordered even in the ground state, which is seemingly unnatural. The other is the state in which each t_{2g} orbital is occupied by one electron. In this picture, the Cr atom becomes trivalent, which reasonably explains the physical properties of $CrSe_2$. The increase of χ likely originates from the change of unclustered Cr valences from +4 to +3, which corresponds to the change of spin from $S = 1$ to $S = 3/2$. The change of ρ is caused by consequently generated holes in the conduction band due to electron transfer to Cr.

Electron transfer from an anion to a transition metal is sometimes observed in compounds with small or negative charge transfer energy in the ZSA scheme [7,8]. Due to the stable Cr^{3+} state, the energy level of the Cr 3*d* band sometimes becomes lower than that of the highest anion *p* band in Cr^{4+} materials such as CrO_2 [9]. For selenides, this tendency is more pronounced because of a wider Se *p* band than O *p* band and smaller electronegativity of Se than that of O. It is reasonable to think that $CrSe_2$ also belongs to negative charge transfer energy materials. Therefore, it is expected that electron transfer from Se to Cr and the formation of Cr^{3+} easily occur in $CrSe_2$.

Increases of χ at both transition temperatures by lowering temperature are reasonably explained by the formation of Cr^{3+} accompanied by electron transfer from Se. This two-step nature is consistent with the structure of the LT phase. In the LT phase, $CrSe_2$ has two unclustered Cr sites, Cr1 and Cr2. Thus, electron transfer from Se to Cr1 and to Cr2 is likely to take place at different temperatures. In this case, χ exhibits two-step increases, namely, successive transitions. Furthermore, we consider that Cr1 and Cr2 likely become trivalent at T_{t1} and T_{t2}, respectively. This is because the magnitude of the jump at T_{t2} is about twice that at T_{t1}, and the number of Cr2 sites is twice as many as that of Cr1 sites.

Considering these successive changes of Cr valence, we propose a possible structure of the IT phase, although we have a relatively small amount of structural information about the IT phase because of a narrow temperature region of about 20 K. From XRD measurements, we have determined that the IT phase has a structure with $a \neq b$ and that its translational symmetry is the same as that of the LT phase. Thus, the symmetry of the IT phase is lower than that of the LT phase, and consequently the space group of the IT phase is a subgroup of trigonal $R\bar{3}m$. Based on the space group relations, the only possible space group of the IT phase is monoclinic $I2/m$ with $\boldsymbol{a}_m = \frac{2}{3}\boldsymbol{a} + \frac{1}{3}\boldsymbol{b} - \frac{1}{3}\boldsymbol{c}$, $\boldsymbol{b}_m = \boldsymbol{b}$, and $\boldsymbol{c}_m = \boldsymbol{c}$, where $\boldsymbol{a}_m$, $\boldsymbol{b}_m$, and $\boldsymbol{c}_m$ are the lattice vectors of this monoclinic structure and $\boldsymbol{a}$, $\boldsymbol{b}$, and $\boldsymbol{c}$ are those of the hexagonal cell of the LT phase. Now we can speculate the orbital ordering pattern of the IT phase. As expected from χ data, Cr1 seems to be trivalent and Cr2 seems to remain tetravalent in the IT phase. In the orbital ordered state of the LT phase, all occupied t_{2g} orbitals of Cr3 point toward Cr2, which indicates that t_{2g} orbitals of Cr2 are ordered in the IT phase. In addition, the IT phase with a $I2/m$ symmetry has one Cr site corresponding to the Cr2 site of the LT phase, and Cr2 has no longer threefold rotation axes but has a mirror plane perpendicular to the $\boldsymbol{b}_m$ axis. Considering the symmetry, an orbital ordering pattern of the IT phase is uniquely determined, as depicted in Fig. 5(c). As a result, the additional formation of bondings through t_{2g} orbitals between Cr2 and Cr3 atoms reduces the in-plane distance between hexamer Cr clusters perpendicular to the *b* axis, which is consistent with our XRD studies.

Interestingly, the LT phase has a higher symmetry than the IT phase even though the temperature region of the LT phase is lower than that of the IT phase. In general, a second-order phase transition is associated with symmetry breaking with decreasing temperature. This can be applied to first-order phase transitions with small structural changes. Indeed, the symmetry of the IT phase of $CrSe_2$ is lower than that of the HT phase. However, in $CrSe_2$, through the transition from the IT phase to the LT phase, a space group changes from lower symmetry $I2/m$ to higher symmetry $R\bar{3}m$. This symmetry change seems unusual, since symmetry restoration occurs with decreasing temperature. The origin of this symmetry restoration is unstable electronic states of Cr^{4+}. Since an orbital ordered Cr^{4+} state of the IT phase is electronically unstable, Cr2 becomes trivalent with lowering temperature, and hence orbital ordering of Cr2 is eliminated, which causes the symmetry restoration from $I2/m$ to $R\bar{3}m$.

Electron transfer and consequent hole doping into the conduction band also have a large influence on ρ. It was reported that the Seebeck coefficient from 5 K to 300 K is positive [3], indicating that the main carriers are holes in the conduction band. Through the transition from the HT phase to the IT phase, the number of holes increases, and as a result, ρ decreases. On the other hand, ρ increases through the transition from the IT phase to the LT phase, indicating a reduction of the number of carriers. This likely originates from complete occupation of a minor band as a result of additional hole doping.

The most characteristic feature of these successive phase transitions in $CrSe_2$ is that they are driven by interplay between orbital degrees of freedom and the electronic instability of Cr in the ZSA scheme. In the HT phase, all Cr atoms are in a tetravalent state without orbital ordering, possessing both orbital degrees of freedom and electronic instability. At T_{t1}, due to cooperative effects between them, orbitals of Cr2 and Cr3 are ordered, and Cr1 becomes trivalent simultaneously. In the triangular lattice at the HT phase, orbitals are not ordered due to the macroscopic degeneracy of orbital states. However, with lattice distortion driven by the formation of Cr^{3+}, this orbital degeneracy is removed and orbitals are ordered. In the IT phase, Cr2 is in a stable orbital ordered state but in an electronically unstable tetravalent state. Hence, the IT phase has competition between orbital ordering and a valence change to Cr^{3+}. At T_{t2}, as a result of this competition, Cr2 becomes a trivalent state without orbital degrees of freedom and, consequently, orbital ordering of Cr2 vanishes. Both cooperation and competition are observed in $CrSe_2$ as two-phase transitions at T_{t1} and T_{t2}, respectively.

IV. SUMMARY

We have prepared pure polycrystalline samples. In addition, we have obtained single crystals of $CrSe_2$. $CrSe_2$ shows successive structural phase transitions at 190 K and 170 K. In the ground state, it has hexamer Cr clusters. Through these phase transitions, t_{2g} orbitals of Cr become ordered, and electrons transfer from Se to Cr, which causes drastic changes of magnetic susceptibility and electrical resistivity. $CrSe_2$ is exotic because of the simultaneous occurrence of orbital ordering and electron transfer.

ACKNOWLEDGMENTS

Inductively coupled plasma spectrometry and electron diffraction measurements were performed using facilities of the Institute for Solid State Physics, the University of Tokyo. We thank M. Koike and M. Isobe for chemical analyses. This

work was partially carried out using facilities of Research Center for Low Temperature and Materials Sciences, Kyoto University. This work was supported by a Grant-in-Aid for Scientific Research from the Japan Society for Promotion of Science (Grant No. 23550152), Grants for Excellent Graduate Schools, MEXT, Japan, and a Grant-in-Aid for Science Research from Graduate School of Science, Kyoto University.

[1] F. J. Di Salvo, D. E. Moncton, and J. V. Waszczak, Phys. Rev. B **14**, 4321 (1976).
[2] K. Tsutsumi, Phys. Rev. B **26**, 5756 (1982).
[3] C. F. van Bruggen, R. J. Haange, G. A. Wiegers, and D. K. G. de Boer, Physica B **99**, 166 (1980).
[4] D. C. Freitas, M. Núñez, P. Strobel, A. Sulpice, R. Weht, A. A. Aligia, and M. Núñez-Regueiro, Phys. Rev. B **87**, 014420 (2013).
[5] S. Chattopadhyay and A. P. Deshpande, J. Phys. Soc. Jpn. **55**, 2320 (1986).
[6] C. M. Fang, C. F. van Bruggen, R. A. de Groot, G. A. Wiegers, and C. Haas, J. Phys.: Condens. Matter **9**, 10173 (1997).
[7] J. Zaanen, G. A. Sawatzky, and J. W. Allen, Phys. Rev. Lett. **55**, 418 (1985).
[8] T. Mizokawa, H. Namatame, A. Fujimori, K. Akeyama, H. Kondoh, H. Kuroda, and N. Kosugi, Phys. Rev. Lett. **67**, 1638 (1991).
[9] M. A. Korotin, V. I. Anisimov, D. I. Khomskii, and G. A. Sawatzky, Phys. Rev. Lett. **80**, 4305 (1998).
[10] B. L. Chamberland, CRC Crit. Rev. Solid State Sci. **7**, 1 (1977).
[11] J. H. Shim, S. Lee, J. Dho, and D. H. Kim, Phys. Rev. Lett. **99**, 057209 (2007).
[12] H. Sakurai, T. Kolodiazhnyi, Y. Michiue, E. Takayama-Muromachi, Y. Tanabe, and H. Kikuchi, Angew. Chem. **124**, 6757 (2012).
[13] K. Hasegawa, M. Isobe, T. Yamauchi, H. Ueda, J. I. Yamaura, H. Gotou, T. Yagi, H. Sato, and Y. Ueda, Phys. Rev. Lett. **103**, 146403 (2009).
[14] Y. Horibe, M. Shingu, K. Kurushima, H. Ishibashi, N. Ikeda, K. Kato, Y. Motome, N. Furukawa, S. Mori, and T. Katsufuji, Phys. Rev. Lett. **96**, 086406 (2006).
[15] M. Isobe and Y. Ueda, J. Phys. Soc. Jpn. **71**, 1848 (2002).
[16] P. G. Radaelli, Y. Horibe, M. J. Gutmann, H. Ishibashi, C. H. Chen, R. M. Ibberson, Y. Koyama, Y. S. Hor, V. Kiryukhin, and S. W. Cheong, Nature (London) **416**, 155 (2002).
[17] D. I. Khomskii and T. Mizokawa, Phys. Rev. Lett. **94**, 156402 (2005).
[18] H. F. Pen, J. van den Brink, D. I. Khomskii, and G. A. Sawatzky, Phys. Rev. Lett. **78**, 1323 (1997).
[19] W. Tian, M. F. Chisholm, P. G. Khalifah, R. Jin, B. C. Sales, S. E. Nagler, and D. Mandrus, Mater. Res. Bull. **39**, 1319 (2004).
[20] N. Katayama, M. Uchida, D. Hashizume, S. Niitaka, J. Matsuno, D. Matsumura, Y. Nishihata, J. Mizuki, N. Takeshita, A. Gauzzi, M. Nohara, and H. Takagi, Phys. Rev. Lett. **103**, 146405 (2009).
[21] Y. Adachi, M. Ohashi, T. Kaneko, M. Yuzuri, Y. Yamaguchi, S. Funahashi, and Y. Mori, J. Phys. Soc. Jpn. **63**, 1548 (1994).
[22] F. J. DiSalvo and J. V. Waszczak, Phys. Rev. B **23**, 457 (1981).
[23] T. Kajita, T. Kanzaki, T. Suzuki, J. E. Kim, K. Kato, M. Takata, and T. Katsufuji, Phys. Rev. B **81**, 060405(R) (2010).